R. & M. No. 2774
(13,452)
A.R.C. Technical Report

MINISTRY OF SUPPLY

AERONAUTICAL RESEARCH COUNCIL
REPORTS AND MEMORANDA

The Effect of Sweepback on the Fundamental Derivative Coefficient for Flexural Motion

By

J. B. BRATT, B.A., B.Sc., and K. C. WIGHT,
of the Aerodynamics Division, N.P.L.

LONDON: HER MAJESTY'S STATIONERY OFFICE
1953
SIX SHILLINGS NET

The Effect of Sweepback on the Fundamental Derivative Coefficient for Flexural Motion

By

J. B. BRATT, B.A., B.Sc., and K. C. WIGHT,
of the Aerodynamics Division, N.P.L.

COMMUNICATED BY THE PRINCIPAL DIRECTOR OF SCIENTIFIC RESEARCH (AIR), MINISTRY OF SUPPLY

*Reports and Memoranda No. 2774**
October, 1950

Summary.—Measurements have been made with new equipment, designed for derivative tests in a 9 × 7 ft tunnel, to determine the effect of sweepback on the derivatives $\lambda_{\dot{\phi}}$ and λ_{ϕ} for a rectangular aerofoil of aspect ratio 6. A numerical reduction was observed in each case, amounting to 15 per cent for $\lambda_{\dot{\phi}}$ and 20 to 30 per cent for λ_{ϕ} over the range $\omega = 1{\cdot}0$ to $1{\cdot}5$ with a sweepback angle of $41{\cdot}3$ deg.

Values of $\lambda_{\dot{\theta}}$ and λ_{θ} for the swept model were obtained from measurements relating to oscillation about an axis perpendicular to the leading edge.

A comparison of $\lambda_{\dot{\phi}}$ and λ_{ϕ} with available theoretical results for finite aspect ratio is made and good agreement observed in the case of the former. The less satisfactory agreement with λ_{ϕ} is thought to be due to the lower accuracy of the theoretical values.

Some difficulty was experienced in the interpretation of the measurements on the swept aerofoil due to distortion of the model during oscillation. The effect is examined in detail in an appendix and a method of correction devised.

A comparison between measurements of $\lambda_{\dot{\phi}}$ for the unswept aerofoil and earlier measurements made with the same model by the method of decaying oscillations gives satisfactory agreement.

1. *Introduction.*—The derivative measurements described in this paper were obtained with the equipment constructed at the National Physical Laboratory for the measurement of forces on oscillating models in a 9 × 7 ft wind tunnel. An existing unswept aerofoil was used as a test model during the development of the apparatus. Since measurements of $\lambda_{\dot{\phi}}$ had already been made on this model by the method of decaying oscillations (R. & M. 2032[1]), results obtained by the two different techniques could be compared.

The swept aerofoil was constructed from an existing unswept model of similar profile, but smaller chord, by addition of suitable tip and root members to give the same aerodynamic chord and aspect ratio as in the unswept case. This resulted in the thickness/chord ratio being reduced to $\frac{3}{4}$ of the value for the latter.

Only a brief account of the equipment and experimental technique is included here, since a detailed description will be given in a separate report.

2. *Description of Apparatus.*—The method of inexorable forcing is used, and the apparatus includes a mechanical oscillator with a number of forcing stations each consisting of an eccentric fitted to a main driving shaft and connected to a point on the model via a linkage system. A special type of balance incorporated in each linkage system measures the instantaneous reaction at the forcing point due to the aerodynamic forces. Provision has been made for ten forcing stations in the completed equipment, which will enable measurements to be made on a flexible

* Published with the permission of the Director, National Physical Laboratory.

model with an imposed mode of deformation. Two stations were available when the present tests were made, one being used for forcing and the other running idle.

Fig. 1 shows a diagrammatic representation of a forcing station. Its position along the shaft is adjustable, the linkage system and balance sliding on I-section steel joists, whilst the eccentric slides along the shaft. Its distance from the shaft can also be altered, but this involves a change in length of the connecting rod between the eccentric and bell-crank. The horizontal lever in the linkage system pivots about point A on the balance to which it transmits the reaction to be measured. Inertial reaction due to the mass of the model and associated fittings is automatically balanced out by the mass M, which is adjusted during a still-air experiment*. Similarly reactions due to springs tensioning the long and slender driving rod are balanced out by spring S. All pivots transmitting load to the balance are constructed in the form of spring bearings in order to avoid the uncertainties of solid friction.

In the earlier experimental work with the unswept wing a development of the automatic electric balance[2] was employed. This was found to be unsatisfactory at the higher frequencies of oscillation, due to overloading by relatively large vibrational reactions of still higher frequency superimposed on the aerodynamic reactions. These extraneous vibrations are thought to be due partly to tunnel vibration and partly to impulses from ball-bearings. A simpler type of balance was finally adopted in which the measuring element consists of a steel strip to which the reactions are applied longitudinally. The resulting small changes in length are made to produce corresponding changes in the width of an optical slit on which the image of a lamp filament is focussed; the variations in intensity of the emergent light are then converted into voltage variations by means of a photocell.

An attempt was made to use resistance-wire strain-gauges cemented to the surfaces of the steel strip, but the stability was found to be inadequate for measuring the very small strains involved. The strain for a given load is determined by the longitudinal stiffness of the strip, which forms a weak link in the system, a lower limit being set to the stiffness by frequency response requirements. With the strip† used in these experiments the estimated frequency response showed a rise of 1 per cent at 10 c.p.s.

Photographs of the equipment are given in Figs. 3 and 4.

The output from the balance is measured in the a.c. bridge circuit shown in Fig. 2, a.c. reference voltages E_1 and E_2 respectively in phase and in quadrature with the motion of the model are provided by two generators consisting of coils oscillated in magnetic fields by the mechanical oscillator. In the present arrangement, which is temporary, the coils are attached to the vertical links between the bell-cranks and horizontal levers in the two forcing stations, the idle station being set 90 degrees out of phase with the driving station. The voltages E_1, E_2 are adjusted by means of voltage dividers and their vector sum balanced against the output E from the strip balance.

The indicator incorporates a high-gain amplifier followed by a cathode-ray tuning indicator, in which oscillation of the shadow angle is produced when the bridge is unbalanced. The preceding filter is essential for the removal of unwanted frequencies, mainly due to extraneous vibrations, which would obscure the balance point. Since conventional inductance-capacity filters are impracticable at the low frequencies of the tests (1 to 10 c.p.s.), an electronic filter is used, which is in effect a tunable amplifier. Tuning is carried out by adjusting resistive components in a twin-T filter included in a negative feedback loop.

The components of aerodynamic reaction can be calculated from the voltage divider settings when the voltages generated by the oscillating coils and the relation between voltage and load for the balance are known. The latter is determined by static loading, the output voltage being measured with an accurate potentiometer. In the case of the coil voltages, these are first

* This automatically subtracts from the reaction measured in the wind a reaction corresponding to the still-air virtual inertia of the model.

† The dimensions of the strip were $3{\cdot}0 \times 0{\cdot}25 \times 0{\cdot}02$ in.

rectified mechanically by means of relays operated from the main drive. The resulting d.c. voltages are then smoothed in a resistance-capacity filter and measured by a null method using a d.c. potentiometer.

Frequency of oscillation is measured with a special type of stroboscope controlled by an accurate 50-cycle tuning fork.

In the tests to be described the amplitude of oscillation was measured with a travelling microscope focussed on a small ball-bearing attached to the link driving the model and illuminated by a distant lamp.

3. *Dynamic Calibration.*—In order to test the behaviour of the apparatus as a whole, measurements were made of the reaction produced by a mass attached to the link connecting the model to the horizontal lever. The unknown effects of additional aerodynamic inertia and aerodynamic damping associated with this mass were eliminated by making repeat measurements with a mass of the same physical dimensions but much reduced density (wood as compared with steel). If the difference between corresponding components of inertial reaction is denoted by δR_1 for the in-phase and δR_2 for the out-of-phase component, and δR_0 is the calculated reaction, the relations $\delta R_1/\delta R_0 = 1$ and $\varepsilon = \tan^{-1} \delta R_2/\delta R_0 = 0$ should be satisfied. Values of $\delta R_1/\delta R_0$ and ε are plotted in Figs. 5a and 5b. For the range of frequency covered the maximum difference between measured and calculated reaction is approximately 2 per cent and the phase is shifted by about $\frac{1}{4}$ degree. Measurements at lower frequencies were not attempted since a larger mass would have been required to give a measurable reaction. It was thought that this might alter the characteristics of the system.

4. *Description of Models.*—The unswept model was a rectangular symmetrical NACA 0015 aerofoil of 60 in. span and 20 in. chord. The swept model was in effect the same aerofoil sheared back through an angle of 41·3 deg and with the thickness/chord ratio reduced by 25 per cent. Both aerofoils were given a rolling oscillation about an axis OX coincident with the root chord and the wind direction (*see* Fig. 6). The swept model was also oscillated about axis OY perpendicular to the leading edge; in which case metal plates for rigidly connecting the outboard to the inboard section were removed, and the latter held fixed by a vertical strut connected to the tunnel structure. Both axes were provided by spring bearings which, in the case of OY, were housed within the profile. The forcing point was situated at a distance of 40 in. from axis OX and lay on the inertia axis appropriate to a two-dimensional aerofoil of the same structure. The attachment to the model was in each case by means of an internal spring bearing, which was made universal for the swept wing in order to allow rotation about either axis.

The aerofoils were hollow wooden structures built up from two spars and a set of ribs with a thin wooden cover. Ribs and spars were lightened as far as was consistent with rigidity.

Photographs of the swept aerofoil mounted in the tunnel are given in Figs. 7 and 8.

5. *Definitions.*—The leading edge is taken as reference axis, with a reference centre R at distance l from axis OX (*see* Fig. 6).

ϕ denotes rotation of R about axis OX (positive for downward displacement)

θ denotes change of incidence at R

y denotes distance from OX of a point on the reference axis

$\eta = y/l$

$l = 0{\cdot}7s$, where s is span

$z(\eta)$, $\theta(\eta)$ denote downward displacement and change of incidence for a point on the reference axis at section η

$z(\eta) = l\phi\, f(\eta)$, $\theta(\eta) = \theta\, F(\eta)$ where $f(\eta)$ and $F(\eta)$ are modal functions

The moment about OX measured at R is given by *

$$L = \phi L_\phi + \dot{\phi} L_{\dot{\phi}} + \theta L_\theta + \dot{\theta} L_{\dot{\theta}} .$$

Since in this case ϕ and θ, when both present, are oscillatory motions in the same phase, the amplitudes of the components of L in phase and in quadrature with the motion are given respectively by

$$L_1 = \bar{\phi} L_\phi + \bar{\theta} L_\theta ,$$
$$L_2 = p(\bar{\phi} L_{\dot{\phi}} + \bar{\theta} L_{\dot{\theta}}),$$

the motions being $\phi = \bar{\phi} e^{jpt}$, $\theta = \bar{\theta} e^{jpt}$. In non-dimensional form these become

$$l_1 = - L_1 / \rho V^2 l^3 \bar{\phi} \int_0^{s/l} f^2 \, d\eta = \lambda_\phi + k\lambda_\theta ,$$

$$l_2 = - L_2 / \rho V l^3 c p \bar{\phi} \int_0^{s/l} f^2 \, d\eta = \lambda_{\dot{\phi}} + k\lambda_{\dot{\theta}}$$

where

l is air density

V is wind speed

c is chord

p is circular frequency

$$k = c\bar{\theta} \int_0^{s/l} fF \, d\eta \Big/ l\bar{\phi} \int_0^{s/l} f^2 \, d\eta$$

and λ_ϕ, $\lambda_{\dot{\phi}}$, λ_θ, $\lambda_{\dot{\theta}}$ are the fundamental equivalent constant leading edge derivative coefficients for the modes under consideration.

For oscillation about axis OX, θ is absent and the mode is linear. The modes† for oscillation about axis OY are shown in Fig. 9, the corresponding value of k being $0 \cdot 2975$.

6. *Apparatus Damping and Inertia Corrections.*—Let $\overline{R}_1$ and $\overline{R}_2$ denote the measured in-phase and in-quadrature reactions at the forcing station. For oscillations in still air it was found impracticable to reduce $\overline{R}_1$ exactly to zero by adjustment of the mass M and spring S referred to in section 2. The small residual value was therefore measured at each frequency and applied as a correction to the value obtained with the tunnel running, the corrected in-phase reaction being denoted by R_1. It should be noted that stiffness derivatives measured with this equipment represent the total in-phase reaction due to aerodynamic forces in the wind stream less a reaction corresponding to still-air virtual inertia.

Values of $\overline{R}_2$ for oscillation in still air are shown plotted against frequency in Fig. 10. Since these curves tend asymptotically to zero with frequency, it is clear that hysteresis damping in spring bearings and tensioning springs was negligible, as this would produce a constant out-of-phase reaction independent of frequency. The reaction was thus regarded as due solely to still-air damping on the aerofoil and driving linkage. It was clear from the geometry of the system that the latter would be small compared with the former, and since the total still-air value was never greater than about 10 per cent of the value obtained with the tunnel running, the apparatus damping was taken to be negligible. The out-of-phase reaction with the tunnel running is denoted by R_2.

7. *Guard Interference.*—The driving rod and tensioning wire shown in Fig. 1 were shielded from the action of the wind by streamlined tubular guards. In the early tests, made with the automatic electric balance, the guards carried horizontal streamlined plates faced with rubber in order to protect the surface of the model in case of a breakage in the linkage system. The

* This is derived from the actual measured moment by the principle of virtual work.

† The mode F introduces a discontinuity in the aerofoil section between Y and OX.

interference was determined by making measurements with dummy guards and plates situated a short distance inboard of the forcing station, the same distance outboard, and in both positions simultaneously. The results were found to be additive, and the effect of the guards at the forcing station was taken to be equal to the mean of the effects at the inboard and outboard positions.

On changing to the steel-strip balance the horizontal plates were removed, as they had been found to have a large effect on λ_ϕ. The method of correction described above could not now be applied, since the effects were no longer additive. The method finally used was to fit telescopic guards at the forcing station and determine the effect of altering the distance of the ends of the guards from the surface of the model. At a fair distance from the model the effect was found to be small and linear with position, whilst close to the surface large non-linear effects were obtained. The latter were taken to result from disturbed flow near the model, and the former from exposure to the wind forces of varying lengths of driving rod and tensioning wire. By extrapolation of the linear range to the surface of the model, results could be obtained free from both interference effects. Corrections to results obtained with the guards in the normal working position are shown in Figs. 11 and 12. $\Delta\lambda_\phi$ was found to be independent of wind speed V, and $\Delta\lambda_{\dot\phi}$ independent of frequency parameter ω over the ranges covered. No corrections were measured for oscillation of the swept wing about axis OY.

8. *Measurements on the Unswept Aerofoil.*—Values of λ_ϕ and $\lambda_{\dot\phi}$ for wind speeds ranging from 40 to 210 ft/sec are shown plotted against ω in Figs. 13 to 16 and tabulated in Tables 1 and 2. The Reynolds number ranges from $0{\cdot}42 \times 10^6$ to $2{\cdot}20 \times 10^6$, and if due allowance is made for experimental scatter, it appears that scale effect is negligible. The amplitude of oscillation $\overline{\phi}$ was approximately $0{\cdot}5$ deg and the mean incidence 0 deg for all the tests made with the inexorable forcing apparatus.

Figs. 13 and 14 compare results obtained with the steel-strip balance and the automatic electric balance. Earlier results for $\lambda_{\dot\phi}$ obtained by the method of decaying oscillations R. & M. 2032) are also included. On the whole the agreement is satisfactory, the greatest discrepancy occurring in the measurements made with the electric balance at small values of ω and the highest wind speed. It is possible that the discrepancy is due to unreliable guard interference corrections, since the electric balance results were obtained with the earlier arrangement of guards carrying horizontal plates adjacent to the model.

9. *Measurements on the Swept Aerofoil.*—9.1. *Effects of Model Distortion.*—Values of $\lambda_{\dot\phi}$ and λ_ϕ calculated from measured reactions for oscillation about axis OX, in the same way as for the unswept aerofoil, are shown in Figs. 17 and 18*. These curves exhibit a marked effect due to wind speed, and since no scale effect had been observed in the unswept case, distortion of the model was suspected.

An approximate determination of the mode of deformation was made by means of a small concave mirror attached to the upper surface of the model at points on a reference axis parallel to the leading edge and passing through the forcing point. The chosen points were roughly at the tip, three-quarter span, mid-span, and quarter-span positions. A beam of light reflected from the mirror passed through a hole in the tunnel roof and was brought to a focus on a translucent paper screen to produce a Lissajous figure which was traced in with pencil and subsequently analysed.

The results of these tests showed that on the reference axis chosen, the slope perpendicular to OX was linear, whilst a torsional mode existed which in general involved a spanwise variation of phase. Modal functions F_1 and F_2 are shown in Fig. 19 as functions of the spanwise co-ordinate η which in this case is made unity at the forcing point. The change of incidence at section η is now given by $\bar\theta(\eta) = F_1\bar\theta_1 + jF_2\bar\theta_2$

* These results are uncorrected for guard interference, which explains the failure of the λ_ϕ-curves to pass through the origin.

where $\bar{\theta}_1$ and $\bar{\theta}_2$ are the amplitudes of incidence change at the forcing point in phase and in quadrature with the ϕ-motion. It was also established experimentally that

$$\bar{\theta}_1 \propto p^2 ,$$
$$\bar{\theta}_2 \propto pV .$$

These results are used in Appendix II to calculate the order of magnitude of the effect on the measured derivatives. No attempt was made to estimate reliable corrections in this way since the derivatives required for this purpose are not known with certainty and an accurate measurement of the distortion mode would have been difficult on account of the smallness of the deflections (in the worst case the incidence change at the tip was roughly $0 \cdot 13$ deg).

The distortion due to sweepback clearly arises from the introduction of much larger coupling reactions between the rolling (ϕ) and pitching (θ) freedoms. In the unswept case for example the inertial coupling was zero, whereas with sweepback it was considerable.

It is shown in Appendix I that for a constant value of ω the measured in-phase and out-of-phase reaction R_1 and R_2 may be expressed in the form

$$\left.\begin{aligned} R_1 &= a_1 x + b_1 x^2 \\ R_2 &= a_2 x + b_2 x^2 \end{aligned}\right\} \quad .. \quad .. \quad .. \quad .. \quad .. \quad .. \quad (1)$$

where $x = V^2$, provided that the forcing frequency is well below the natural frequency associated with the θ-motion and the direct aerodynamic reactions affecting this displacement are small compared with the elastic reactions. It is assumed that elastic cross-stiffnesses are absent. The terms involving x represent the reactions which would be obtained with no distortion of the model, and these were determined by cross-plotting measured values of R_1 and R_2 against x for constant ω and fitting curves of the form (1) by the method of least squares. Values of a_1 and a_2 were derived directly from the analyses. Satisfactory agreement between the experimental points and least square curves was obtained, and this is regarded as sufficient evidence for the validity of the method of correction employed. The experimental points and least-square curves for $\omega = 0 \cdot 4$ are shown in Fig. 20.

9.2. *Results for Oscillation about Axis OX.*—Values of λ_ϕ and $\lambda_{\dot{\phi}}$ corrected for guard interference and model distortion in the way described above are tabulated in Table 3 and included in Figs. 15 and 16 for comparison with the unswept case. The main effect of the sweepback on these derivative coefficients is a numerical reduction of order 15 per cent for $\lambda_{\dot{\phi}}$ and 20 to 30 per cent for λ_ϕ over the range of $\omega = 1 \cdot 0$ to $1 \cdot 5$.

9.3. *Results for Oscillation about Axis OY.*—No attempt was made to measure guard interference in this case, since its determination involved a large number of measurements, and the previous tests had indicated that the effect is small in the practical range of ω. Corrections for model distortion were obtained in the same way as for axis OX.

Values of $l_2 = \lambda_{\dot{\phi}} + k\lambda_{\dot{\theta}}$ and $l_1 = \lambda_\phi + k\lambda_\theta$, where $k = 0 \cdot 2975$, are plotted against ω in Figs. 21 and 22 and tabulated in Table 4. The value of l_1 for $\omega = 0$ was obtained by harmonic analysis of curves of static reaction at the forcing point plotted against phase setting of the mechanical oscillator for different values of wind speed.

9.4. *Values of λ_θ and $\lambda_{\dot{\theta}}$.*—The cross-derivatives λ_θ and $\lambda_{\dot{\theta}}$ are derivable from the quantities l_1 and l_2 of the previous section if the corresponding direct derivatives λ_ϕ and $\lambda_{\dot{\phi}}$ are known. Values of the latter appropriate to oscillation about axis OX and uncorrected for guard interference have been used to obtain the values of λ_θ and $\lambda_{\dot{\theta}}$ given in Figs. 23 and 24, and Table 5. It is assumed here that the effect on the direct derivative coefficients of the difference in mode for the two axis positions is negligible.

Included in Fig. 24 is a single value of λ_θ for $\omega = 0$ derived from measurements of C_l, the rolling moment about axis OX due to pitch, described in the following section. The relationship used is $\lambda_\theta = \partial C_l / \partial \theta$. This result is about 10 per cent greater than that for rotation about axis OY.

10. *Measurements of C_l.*—For these tests the incidence of the model was altered by rotation about an axis perpendicular to OX and passing through the forcing point. The rolling moment about OX was determined for each incidence from measurements of the reaction at the forcing point for a number of wind speeds, and the result corrected for model distortion in the manner already described for the oscillatory case*.

A curve of C_l plotted against θ is given in Fig. 25, where C_l is defined by the relation $L = \frac{1}{2}\rho V^2 s^2 c\, C_l$. A theoretical curve for 45-deg sweepback is included for comparison, based on solution 13 of R. & M. 2596[3] by Falkner.

11. *Comparison with Theory.*—Mean experimental curves of $\lambda_{\dot{\phi}}$ and λ_{ϕ} are compared with theoretical results in Figs. 26 to 29. Values calculated by Miss D. E. Lehrian (Current Paper No. 51[4]) using a general method for any plan form due to W. P. Jones (R. & M. 2470[5]) are included in Figs. 26 and 27. This method is based on a combination of a theoretical treatment by Jones and a form of Falkner's scheme for the calculation of normal induced velocity due to simple doublet distributions. Its main advantage in comparison with earlier methods is a considerable reduction in the computational labour involved, particularly for wings of constant chord.

The agreement with experiment in the case of $\lambda_{\dot{\phi}}$ is very good for $\omega > 0{\cdot}5$, both for the unswept and swept aerofoils. The values for λ_{ϕ} show best agreement for the swept aerofoil, the results for the unswept aerofoil being low. This may be due to inaccuracies in the calculations, since the separation of λ_{ϕ} from the still-air virtual inertia term involves a small difference of two large quantities.

A comparison is made in Figs. 28 and 29 with earlier results calculated by W. P. Jones (R. & M. 2142[6]) using an approximate method for unswept rectangular wings. The agreement here is satisfactory in the case of the damping, and is better for the stiffness derivative λ_{ϕ} if the symmetrical modes are compared. It is clear from a consideration of the image system in the tunnel walls that this is the appropriate mode.

Curves of theoretical two-dimensional derivative coefficients are also included in the figures. Over the range $\omega = 0{\cdot}5$ to $1{\cdot}5$ the experimental values of $\lambda_{\dot{\phi}}$ for the unswept and swept aerofoils are roughly 66 per cent and 56 per cent respectively of the two-dimensional values. For the same range of ω the value of λ_{ϕ} varies from 50 per cent to 80 per cent of the two-dimensional value approximately in the case of the unswept aerofoil and from 30 per cent to 60 per cent for the swept aerofoil.

The curves of $\lambda_{\dot{\theta}}$ and λ_{θ} in Figs. 23 and 24 are compared with two-dimensional theory. In this case no theoretical values for finite aspect-ratio and the appropriate mode were available.

12. *Conclusions.*—The effect of sweepback on the derivatives $\lambda_{\dot{\phi}}$ and λ_{ϕ} is to produce a reduction in magnitude, which in the present case amounts to 15 per cent for damping and 20 to 30 per cent for stiffness over the range $\omega = 1{\cdot}0$ to $1{\cdot}5$.

The agreement with theory is satisfactory for $\lambda_{\dot{\phi}}$, both as regards the effect of aspect-ratio and sweepback. It is possible that the agreement for λ_{ϕ} would be improved if more accurate calculations were made.

An important result of the tests on the swept wing is the demonstration of the serious effect which model distortion can have on the measurements. It is emphasized that the possibility of errors from this cause should always be borne in mind in derivative measurements when an apparent scale effect is observed.

An incidental result of the tests on the unswept wing is the comparison of measurements of $\lambda_{\dot{\phi}}$ with earlier measurements made by the method of decaying oscillations. Satisfactory agreement is obtained.

---

* It is clear that the error in the reaction due to twist is proportional to the latter, which is itself proportional to aerodynamic loading, *i.e.*, to V_2. This leads to a relation between reaction and wind speed indentical with (1) in section 9.1.

APPENDIX I

Errors in Measurements of L_ϕ and $L_{\dot\phi}$ Due to Torsion

The determinantal equation for the system used in making the measurements may be written

$$\begin{vmatrix} \sigma_\varphi - p^2 I_\phi - L_\phi - jpL_{\dot\phi} + (r_1 + jr_2), & \sigma_1 - p^2 P - L_\theta - jpL_{\dot\theta} \\ \sigma_1 - p^2 P - M_\phi - jpM_{\dot\phi}, & \sigma_\theta - p^2 I_\theta - M_\theta - jpM_{\dot\theta} \end{vmatrix} = 0 , \quad \ldots \quad (2)$$

where I_ϕ, I_θ, σ_ϕ, σ_θ are inertias and direct elastic stiffnesses appropriate to the ϕ and θ-freedoms, and P, σ are product of inertia and elastic cross-stiffness respectively. The conventional notation is used for the derivative coefficients. r_1 and r_2 represent the in-phase and out-of-phase components of the forcing reaction per unit amplitude. The measured reactions R_1 and R_2 of section 9(i) are given in terms of these by

$$\left.\begin{aligned} R_1 &= (r_1 - r_1')\overline{\phi} , \\ R_2 &= r_2\overline{\phi} , \end{aligned}\right\} \quad \ldots \quad (3)$$

where r_1' relates to oscillation in still air.

If it is assumed that for oscillation in still air the aerodynamic reactions are negligible compared with the elastic and inertial reactions, it follows from (2) that the still-air forcing reaction r_1' is given by

$$\begin{vmatrix} \sigma_\phi - p^2 I_\phi + r_1', & \sigma_1 - p^2 P \\ \sigma_1 - p^2 P, & \sigma_\theta - p^2 I_\theta \end{vmatrix} = 0 . \quad \ldots \quad (4)$$

r_1' exceeds the reaction which would be obtained with the θ-freedom absent by an amount $\delta r_1'$ where

$$r_1' - \delta r_1' = -(\sigma_\phi - p^2 I_\phi) , \quad \ldots \quad (5)$$

thus from (4)

$$\begin{vmatrix} \delta r_1', & \sigma_1 - p^2 P \\ \sigma_1 - p^2 P, & \sigma_\theta - p^2 I_\theta \end{vmatrix} = 0 . \quad \ldots \quad (6)$$

The method of measurement described in the main text leads to the relations

$$r_1 - r_1' = L_\phi + \delta L_\phi , \quad \ldots \quad (7)$$

$$r_2 = p(L_{\dot\phi} + \delta L_{\dot\phi}) , \quad \ldots \quad (8)$$

where δL_ϕ, $\delta L_{\dot\phi}$ are the errors in the derivative measurements due to the unwanted freedom. Substitution from (5), (7) and (8) in (2) leads to

$$\begin{vmatrix} \delta L_\phi + \delta r_1' + jp\delta L_{\dot\phi} , & \sigma_1 - p^2 P - L_\theta - jpL_{\dot\theta} \\ \sigma_1 - p^2 P - M_\phi - jpM_{\dot\phi}, & \sigma_\theta - p^2 I_\theta - M_\theta - jpM_{\dot\theta} \end{vmatrix} = 0 , \quad \ldots \quad (9)$$

which together with (6) enables the errors to be determined. These may be written in the form

$$\delta l_\phi + j\omega\delta l_{\dot\phi} = \frac{\left(\frac{\sigma_1}{\rho V^2 l^3} - \omega^2 \frac{P}{\rho c^2 l^3} - l_\theta - j\omega l_{\dot\theta}\right)\left(\frac{\sigma_1}{\rho V^2 l^3} - \omega^2 \frac{P}{\rho c^2 l^3} - m_\phi - j\omega m_{\dot\phi}\right)}{\frac{\sigma_\theta}{\rho V^2 l^3}\left(1 - \frac{p^2}{p_\theta^2}\right) - m_\theta - j\omega m_{\dot\theta}}$$

$$- \frac{\left(\frac{\sigma_1}{\rho V^2 l^3} - \omega^2 \frac{P}{\rho c^2 l^3}\right)^2}{\frac{\sigma_\theta}{\rho V^2 l^3}\left(1 - \frac{p^2}{p_\theta^2}\right)} \quad \ldots \quad (10)$$

where l_ϕ, $l_{\dot\phi}$, m_θ, $m_{\dot\theta}$, etc., are non-dimensional forms of the derivative coefficients, and p_θ is the natural circular frequency for torsion with the ϕ-motion suppressed.

If p is small compared with p_θ, and the direct torsional aerodynamic moments are small compared with the corresponding elastic moment, the right-hand side of (10) has the common denominator $\sigma_\theta/\rho V^2 l^3$. Hence if the elastic cross-stiffness σ_1 is zero

$$\delta l_\phi + j\omega\delta l_{\dot\phi} = \frac{\rho V^2 l^3}{\sigma_\theta}\left[(l_\theta + j\omega l_{\dot\theta})\,(m_\phi + j\omega m_{\dot\phi}) + \frac{\omega^2 P}{\rho c^2 l^3}\left\{(l_\theta + m_\phi) + j\omega(l_{\dot\theta} + m_{\dot\phi})\right\}\right]. \qquad (11)$$

Thus for constant ω the errors in the measurements of the non-dimensional in-phase and out-of-phase aerodynamic reactions are proportional to V^2.

It follows therefore, that with constant ω the measured reactions R_1 and R_2 will be of the form

$$\left.\begin{aligned} R_1 &= (L_\phi + \delta L_\phi)\overline{\phi} = (a_1 + b_1 x)x \\ R_2 &= p(L_{\dot\phi} + \delta L_{\dot\phi})\overline{\phi} = (a_2 + b_2 x)x \end{aligned}\right\}, \qquad (12)$$

where $x = V^2$. These expressions are of the same form as (1) in section 9.1.

The spanwise variation of phase mentioned in section 9.1 appears at first sight to complicate the problem. It may be shown, however, that the relations (12) still hold. For the purpose of setting up the dynamical equations, θ is replaced by independent displacements θ_1 and θ_2 associated with the modal functions F_1 and F_2 of Fig. 19 and the problem treated as for three degrees of freedom. A solution of the form

$$\left.\begin{aligned} \phi &= \overline{\phi}e^{jpt}, \\ \theta_1 &= \overline{\theta}_1 e^{jpt}, \\ \theta_2 &= j\overline{\theta}_2 e^{jpt}, \end{aligned}\right\} \qquad (13)$$

is introduced, where $\overline{\phi}$, $\overline{\theta}_1$, $\overline{\theta}_2$ are real.

From the resulting equations it may be seen that if the torsional aerodynamic moments relating to θ_1 are small compared with the corresponding elastic and inertial reactions, and p is small compared with p_θ, which now represents the natural frequency for the θ_1 motion, then

$$\overline{\theta}_1 \propto p^2. \qquad (14)$$

Also, if in addition the direct torsional damping moment relating to θ_1 is small compared with the torsional moment due to rate of roll, *i.e.*,

$$pM_{\dot\theta_1}\overline{\theta}_1 << pM_{\dot\phi}\overline{\phi}, \qquad (15)$$

then for constant ω

$$\overline{\theta}_2 \propto pV \qquad (16)$$

Condition (15) will be satisfied if $\overline{\theta}_1$ is very small. It was verified for the conditions of the experiment by using measured amplitudes, and derivatives based on two-dimensional theory. The relations (14) and (16) agree with the experimental results given in 9.1, the only difference being that the experimental relation for $\overline{\theta}_2$ is independent of ω. This implies that $M_{\dot\phi}$ in (15) is constant over the range of ω covered.

It follows from (14) and (16) that for constant ω

$$\frac{\overline{\theta}_1}{\overline{\theta}_2} \propto \frac{p}{V} \propto \omega = \text{a constant}. \qquad (17)$$

This implies that for a given ω the problem may be regarded as involving two degree of freedom only, and hence the expressions (12) are applicable.

APPENDIX II

Approximate Calculation of Errors

The three-degree of freedom treatment outlined in Appendix I leads to the equations

$$\left.\begin{aligned} \delta L_\phi &= L_{\theta_1}\frac{\bar{\theta}_1}{\bar{\phi}} - pL_{\dot{\theta}_2}\frac{\bar{\theta}_2}{\bar{\phi}} \\ p\delta L_{\dot{\phi}} &= (p^2P_2 + L_{\theta_2})\frac{\bar{\theta}_2}{\bar{\phi}} + pL_{\dot{\theta}_1}\frac{\bar{\theta}_1}{\bar{\phi}} \end{aligned}\right\}, \quad .. \quad .. \quad .. \quad .. \quad .. \quad .. \quad (18)$$

where L_{θ_1}, $L_{\dot{\theta}_1}$, L_{θ_2}, $L_{\dot{\theta}_2}$ are the derivative coefficients relating to flexual moments produced by θ_1 and θ_2-motions, and P_2 is the product of inertia between the θ_2 and ϕ-motions. Values for the derivatives were calculated on the basis of two-dimensional theory using the modal functions given in Fig. 19. A value for P_2 was obtained from the approximate relation

$$p^2P_2\bar{\theta}_2 = pM_{\dot{\phi}}\bar{\theta}_1 , \quad .. \quad .. \quad .. \quad .. \quad .. \quad .. \quad .. \quad .. \quad .. \quad (19)$$

which results from the assumptions leading to (14) and (16) in Appendix I. The derivative $M_{\dot{\phi}}$ in (19) relates to the θ_1-motion, and it was calculated on the same basis as those in (18).

Values of $\delta\lambda_\phi$ and $\delta\lambda_{\dot{\phi}}$ calculated by substituting measured amplitudes in (18) are tabulated below and compared with measured values of the errors. These are obtained as differences between corrected and uncorrected measurements of the derivatives.

ω	$\delta\lambda_\phi/V^2$		$\delta\lambda_{\dot{\phi}}/V^2$	
	Calculated	Measured	Calculated	Measured
0·4	$2{\cdot}30 \times 10^{-6}$	$2{\cdot}45 \times 10^{-6}$	$7{\cdot}50 \times 10^{-6}$	$6{\cdot}13 \times 10^{-6}$
1·0	10·29 ,,	15·9 ,,	13·16 ,,	10·9 ,,
1·6	23·75 ,,	37·0 ,,	26·16 ,,	13·9 ,,

It seems clear from these results that the distortion of the model would be expected to produce effects of the same order of magnitude as those observed. The differences between calculated and measured values of the errors are no doubt due to the very approximate nature of the data used in the calculations.

REFERENCES

No.	*Author*	*Title, etc.*
1	J. B. Bratt and C. J. Davis ..	The Influence of Aspect Ratio and Taper on the Fundamental Damping Derivative Coefficient for Flexural Motion. R. & M. 2032. February, 1945.
2	J. B. Bratt and K. C. Wight ..	The Development of an Automatic Electric Balance for Research on Aerodynamic Stability. *Phil. Mag.*, Ser. 7, Vol. XXXV, p. 588. September, 1944.
3	V. M. Falkner	Calculated Loadings due to Incidence of a Number of Straight and Swept-back Wings. R. &. M. 2596. June, 1948.
4	D. E. Lehrian	Calculation of the Damping for Rolling Oscillations of a Swept Wing. Current Paper No. 51. October, 1950.
5	W. P. Jones	The Calculation of Aerodynamic Derivative Coefficients for Wings of any Plan Form in Non-Uniform Motion. R. & M. 2470. December, 1946.
6	W. P. Jones	Theoretical Air-load Derivative Coefficients for Rectangular Wings. R. & M. 2142. February, 1943.

TABLE I

Values of $\lambda_{\dot{\phi}}$ for the Unswept Aerofoil

$V = 40$ ft/sec		$V = 80$ ft/sec		$V = 160$ ft/sec		$V = 210$ ft/sec	
ω	$\lambda_{\dot{\phi}}$	ω	$\lambda_{\dot{\phi}}$	ω	$\lambda_{\dot{\phi}}$	ω	$\lambda_{\dot{\phi}}$
0·268	1·401	0·132	1·199	0·066	1·560	0·050	1·478
0·536	1·321	0·263	1·482	0·132	1·561	0·100	1·562
0·803	1·256	0·397	1·401	0·198	1·502	0·150	1·543
1·071	1·220	0·527	1·360	0·264	1·498	0·200	1·520
1·339	1·193	0·659	1·322	0·329	1·454	0·249	1·512
1·604	1·171	0·790	1·279	0·400	1·448	0·304	1·486
1·871	1·160	0·922	1·250	0·460	1·434	0·355	1·475
2·138	1·117	1·054	1·228	0·532	1·395	0·405	1·456
2·406	1·097	1·186	1·227	0·596	1·375	0·451	1·430
2·673	1·075	1·318	1·205	0·663	1·353	0·500	1·428

TABLE 2

Values of λ_{ϕ} for the Unswept Aerofoil

$V = 40$ ft/sec		$V = 80$ ft/sec		$V = 160$ ft/sec		$V = 210$ ft/sec	
ω	λ_{ϕ}	ω	λ_{ϕ}	ω	λ_{ϕ}	ω	λ_{ϕ}
0·268	0·036	0·132	0·036	0·066	0·030	0·050	0·018
0·536	0·155	0·263	0·067	0·132	0·040	0·100	0·037
0·803	0·238	0·397	0·112	0·198	0·061	0·150	0·051
1·071	0·290	0·527	0·154	0·264	0·079	0·200	0·063
1·339	0·374	0·659	0·202	0·329	0·105	0·249	0·083
1·604	0·471	0·790	0·231	0·400	0·127	0·304	0·095
1·871	0·559	0·922	0·279	0·460	0·147	0·355	0·115
2·138	0·671	1·054	0·314	0·532	0·173	0·405	0·137
2·406	0·824	1·186	0·363	0·596	0·202	0·451	0·151
2·673	0·961	1·318	0·411	0·663	0·214	0·500	0·168

TABLE 3

Values of λ_{ϕ} and $\lambda_{\dot{\phi}}$ for the Swept Aerofoil

ω	λ_{ϕ}	$\lambda_{\dot{\phi}}$	ω	λ_{ϕ}	$\lambda_{\dot{\phi}}$
0	0				
0·1	0·005	1·245	0·9	0·199	1·071
0·2	0·013	1·228	1·0	0·223	1·051
0·3	0·038	1·199	1·1	0·241	1·029
0·4	0·056	1·170	1·2	0·264	1·017
0·5	0·075	1·159	1·3	0·290	1·009
0·6	0·123	1·139	1·4	0·330	1·038
0·7	0·150	1·123	1·5	0·371	1·019
0·8	0·180	1·105	1·6	0·402	0·990

TABLE 4

Values of l_1 and l_2 for the Swept Aerofoil (Axis OY)

ω	l_1	l_2	ω	l_1	l_2
0	0·514		0·9	0·653	↑
0·1	0·520	1·470	1·0	0·676	
0·2	0·525	↑	1·1	0·709	
0·3	0·526		1·2	0·737	Constant
0·4	0·542	Constant	1·3	0·746	
0·5	0·551		1·4	0·853	
0·6	0·597		1·5	0·894	
0·7	0·627		1·6	0·912	↓
0·8	0·652	↓			

TABLE 5

Values of λ_θ and $\lambda_{\dot{\theta}}$ for the Swept Aerofoil

ω	λ_θ	$\lambda_{\dot{\theta}}$	ω	λ_θ	$\lambda_{\dot{\theta}}$
0	1·773	0·735	0·9	1·525	1·322
0·1	1·720	0·826	1·0	1·514	1·393
0·2	1·713	0·911	1·1	1·511	1·454
0·3	1·697	0·978	1·2	1·521	1·518
0·4	1·667	1·049	1·3	1·555	1·558
0·5	1·633	1·120	1·4	1·616	1·568
0·6	1·612	1·187	1·5	1·687	1·562
0·7	1·575	1·258	1·6	1·767	1·552
0·8	1·552				

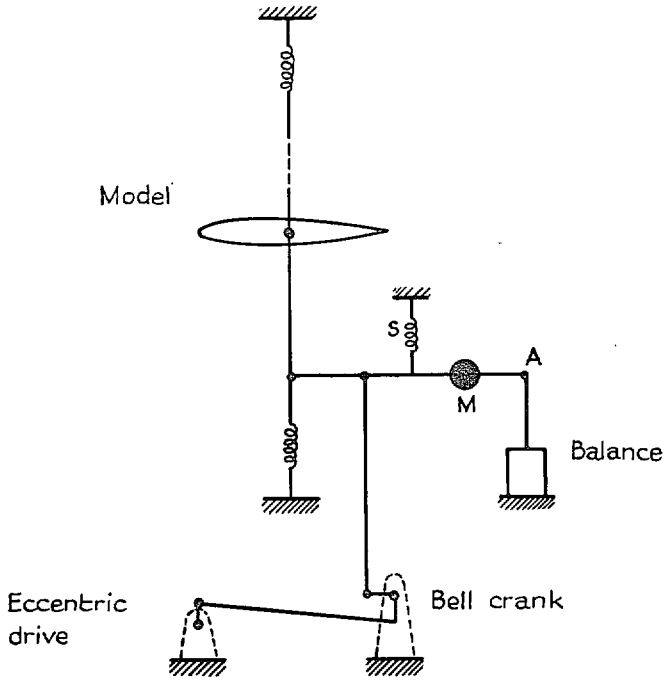

FIG. 1. Diagram of forcing station.

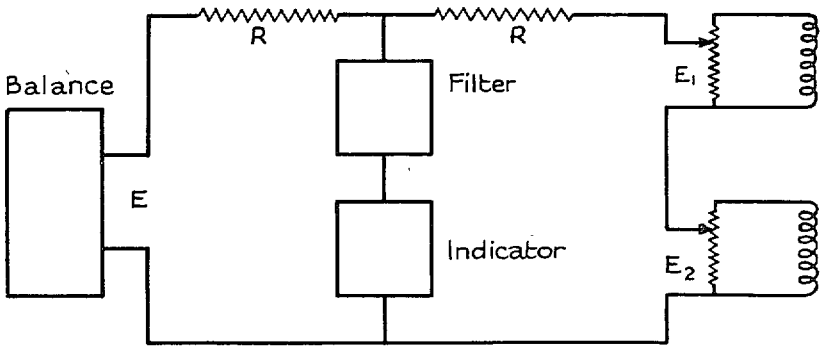

FIG. 2. Alternating current bridge circuit.

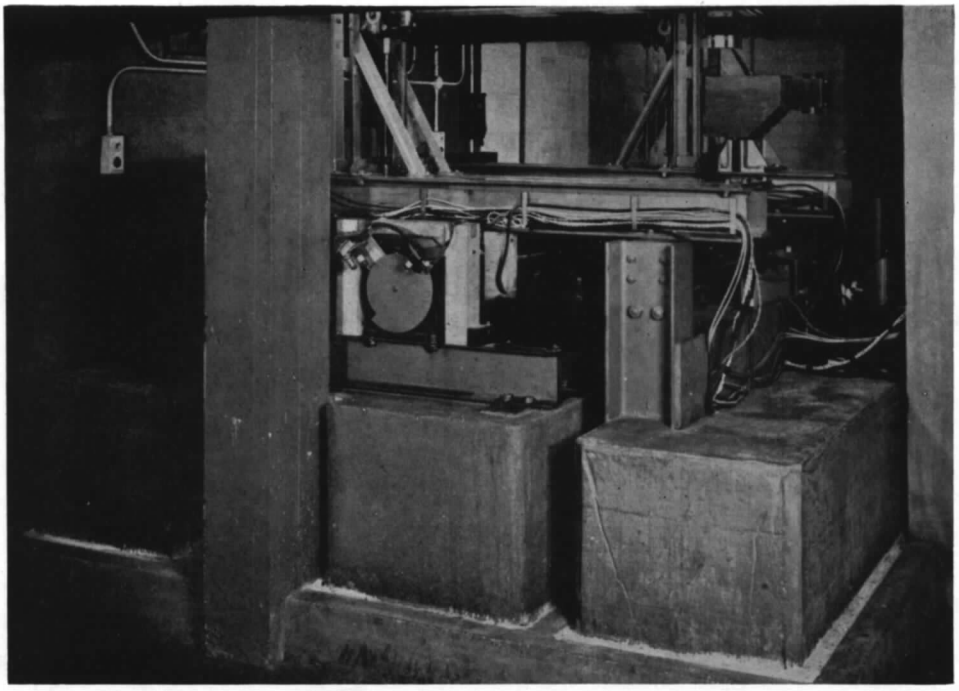

FIG. 3. Mechanical oscillator.

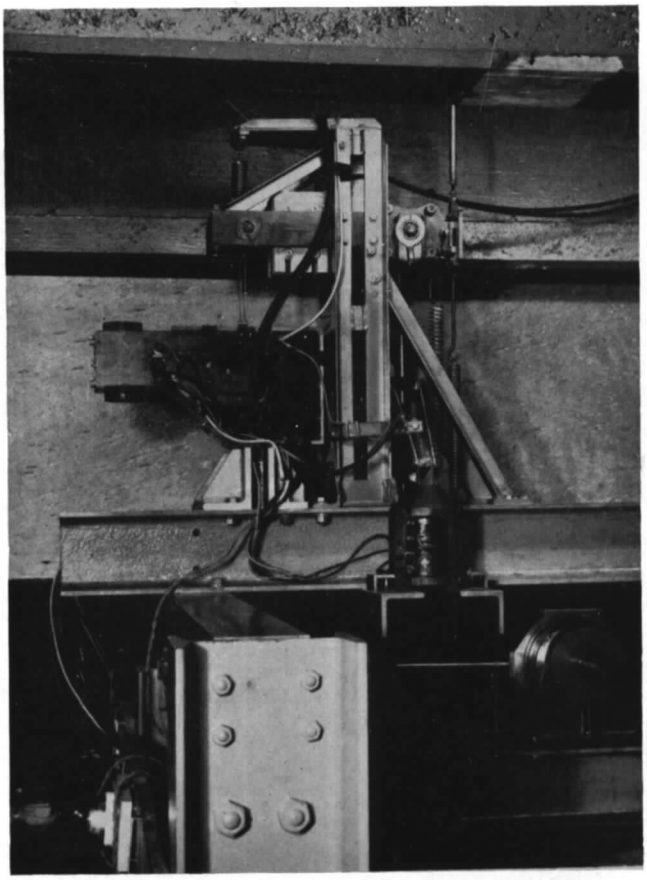

FIG. 4. Forcing station with balance.

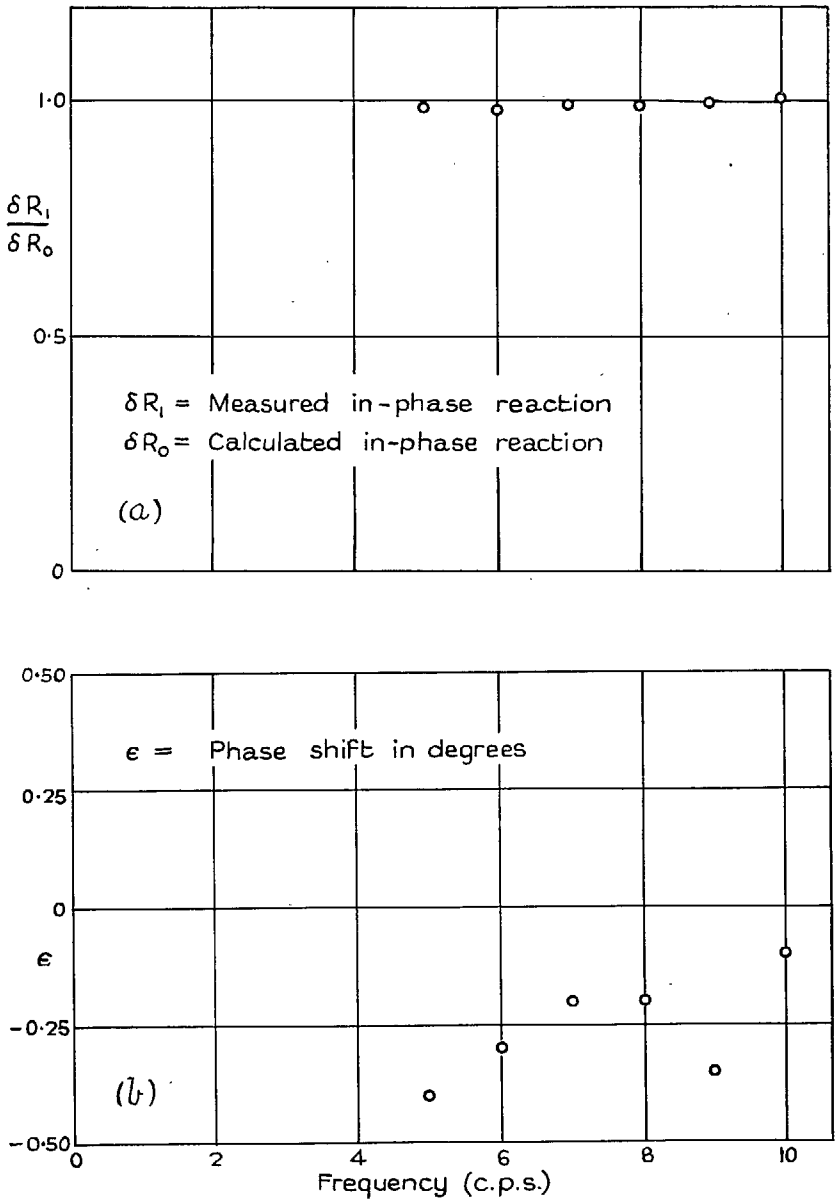

FIG. 5. Dynamic calibration.

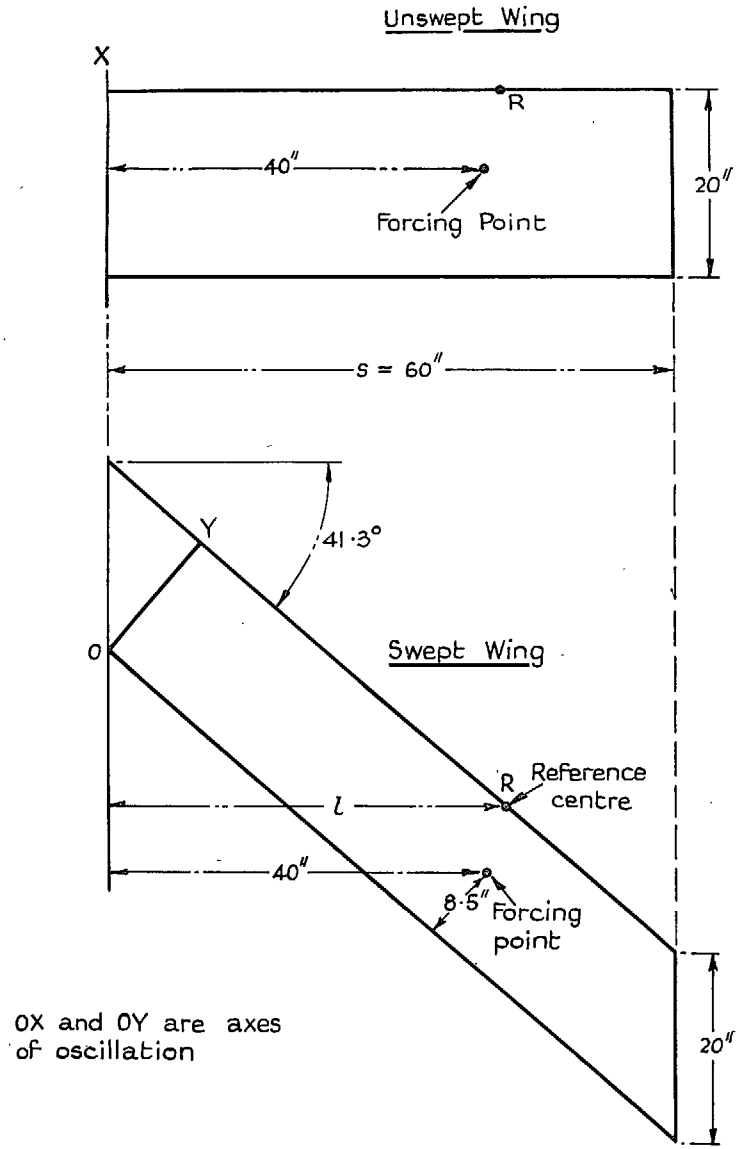

FIG. 6. Planform of aerofoils.

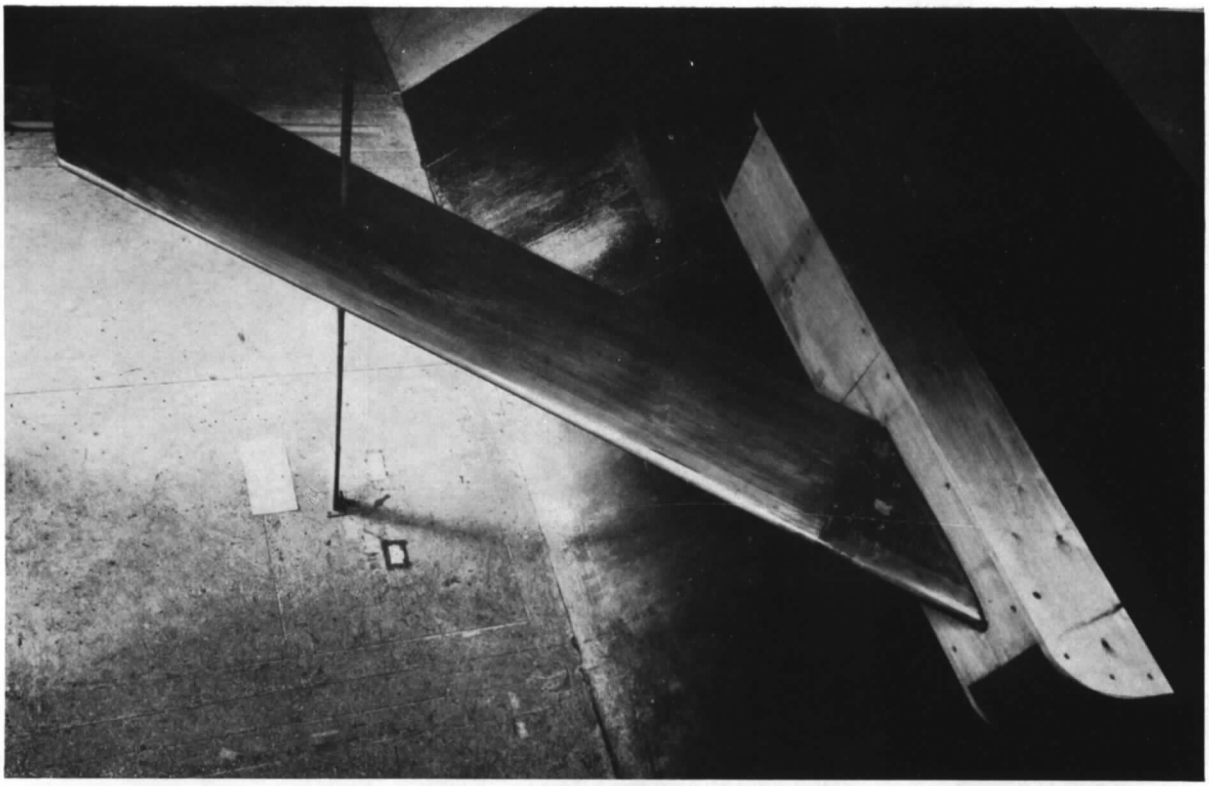

FIG. 7. View of swept wing from below.

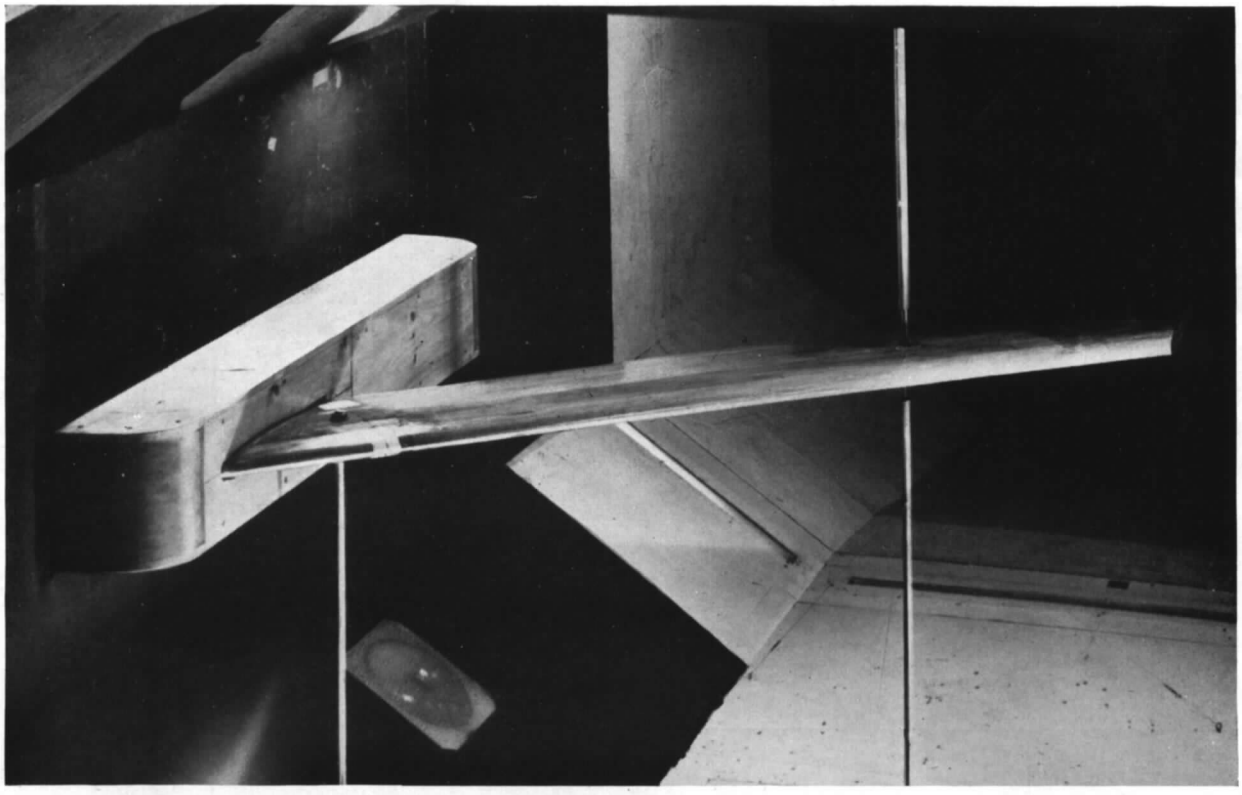

FIG. 8. View of swept wing from above.

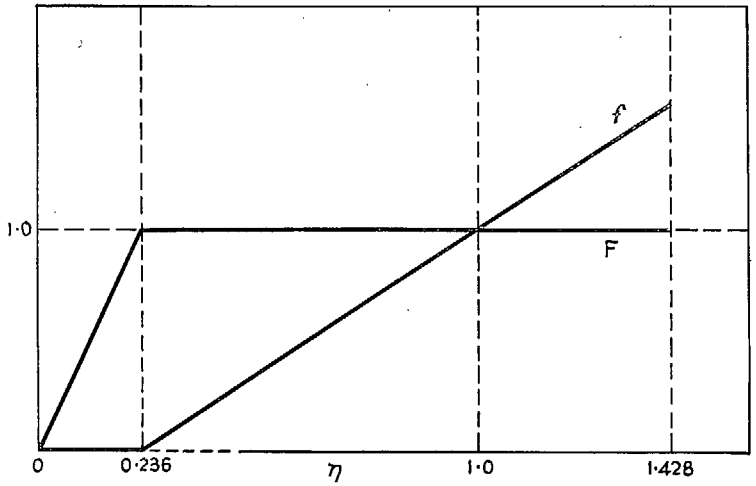

FIG. 9. Modal functions for oscillation about OY (swept aerofoil).

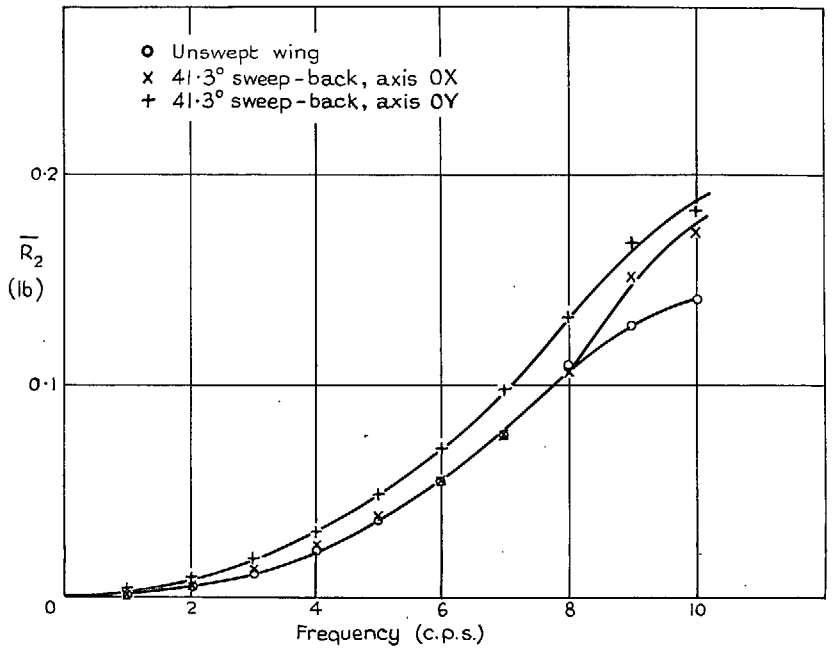

FIG. 10. Dependence of still air damping on frequency.

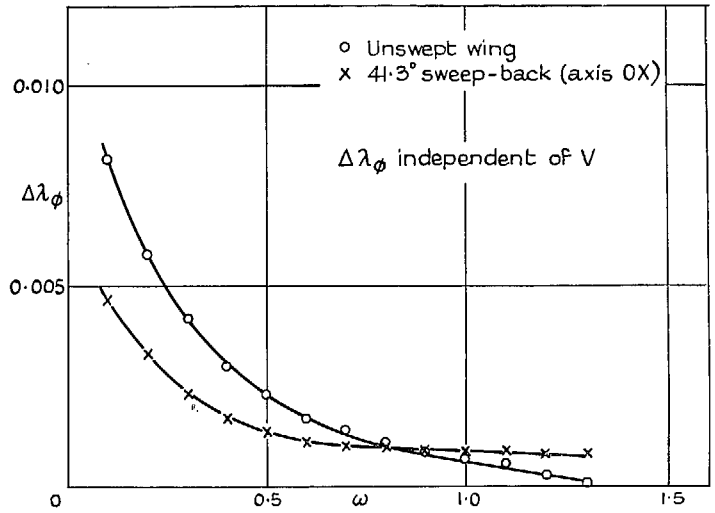

FIG. 11. Corrections to λ_ϕ for guard interference.

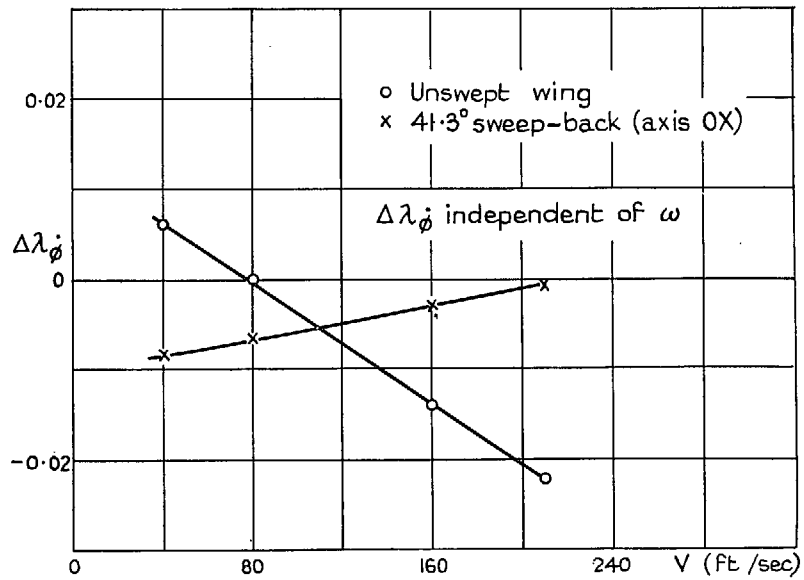

FIG. 12. Corrections to $\lambda_{\dot\phi}$ for guard interference.

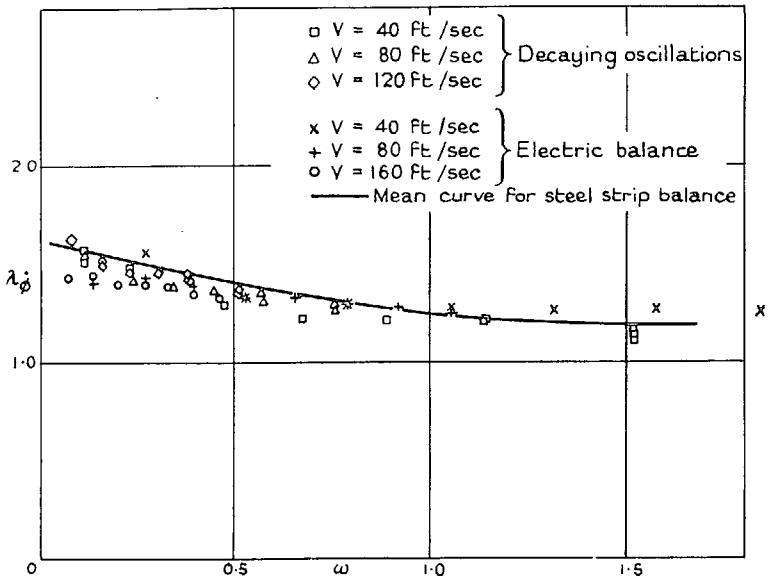

FIG. 13. Comparison of steel-strip and electric balances with decaying oscillation method.

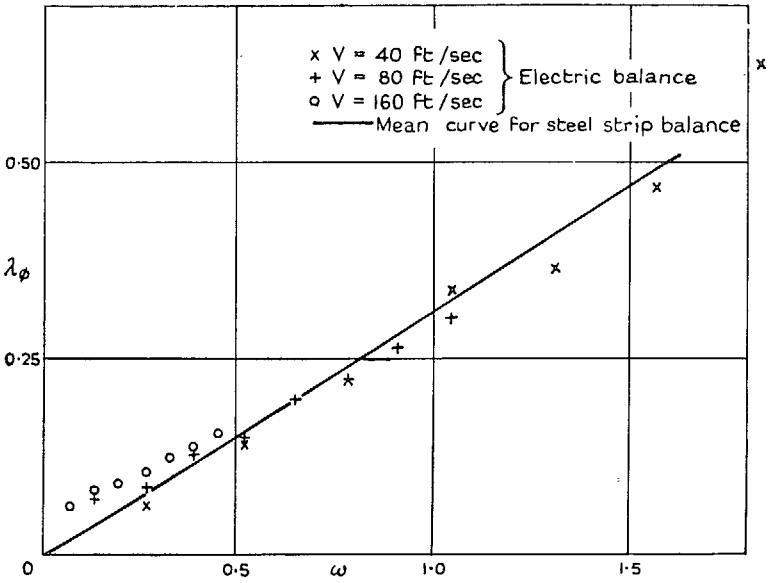

FIG. 14. Comparison of steel-strip and automatic electric balances.

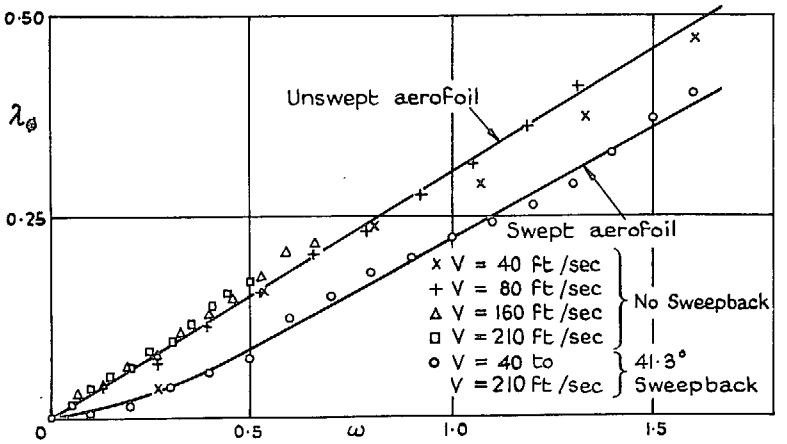

FIG. 15. Dependence of $\lambda_{\dot{\phi}}$ on ω for swept and unswept aerofoils.

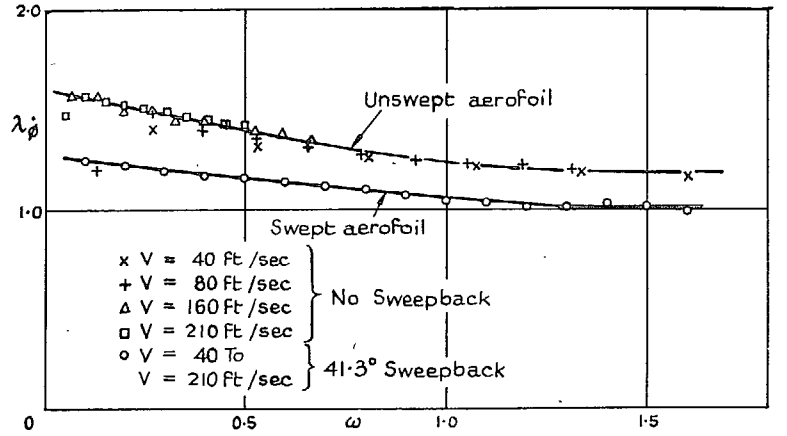

FIG. 16. Dependence of λ_{ϕ} on ω for swept and unswept aerofoils.

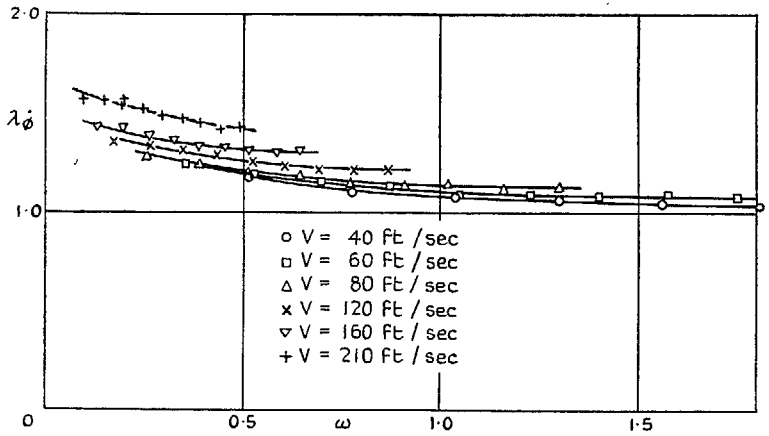

FIG. 17. Effect of model distortion on $\lambda_{\dot{\phi}}$ (swept aerofoil).

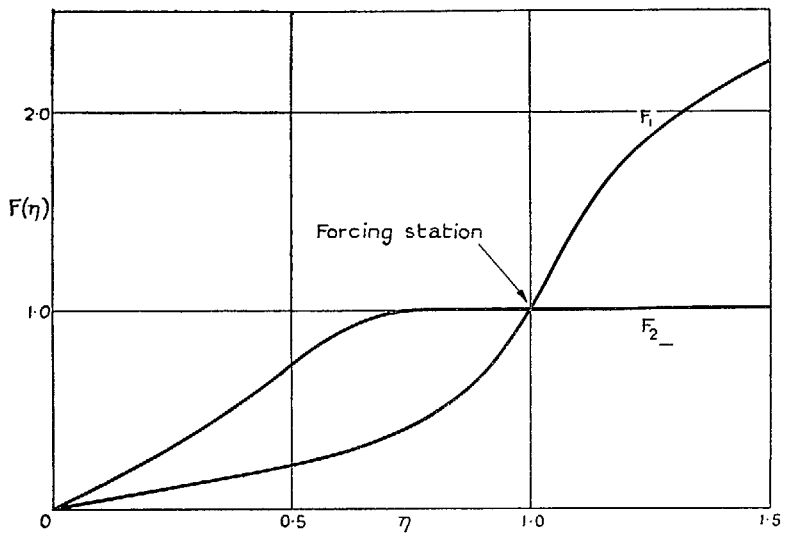

FIG. 19. Distortion modes for swept aerofoil (axis OX).

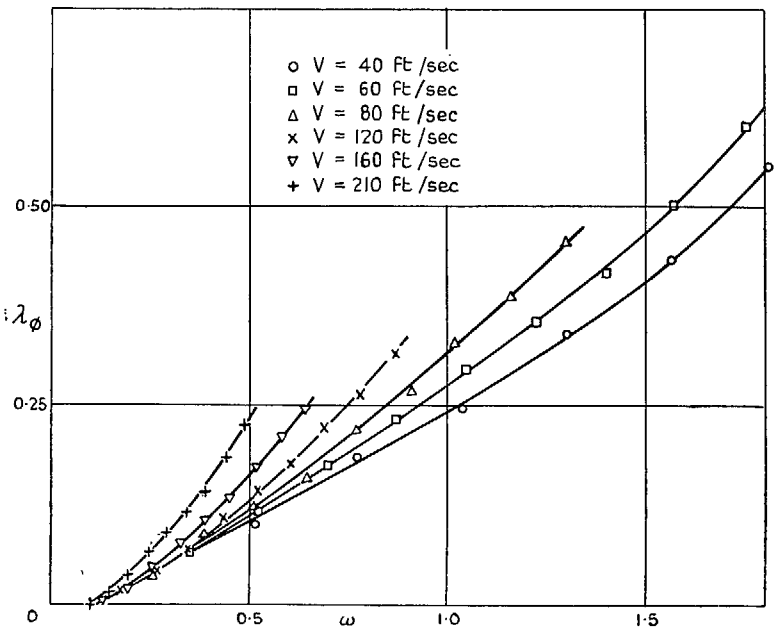

FIG. 18. Effect of model distortion on λ_{ϕ} (swept aerofoil).

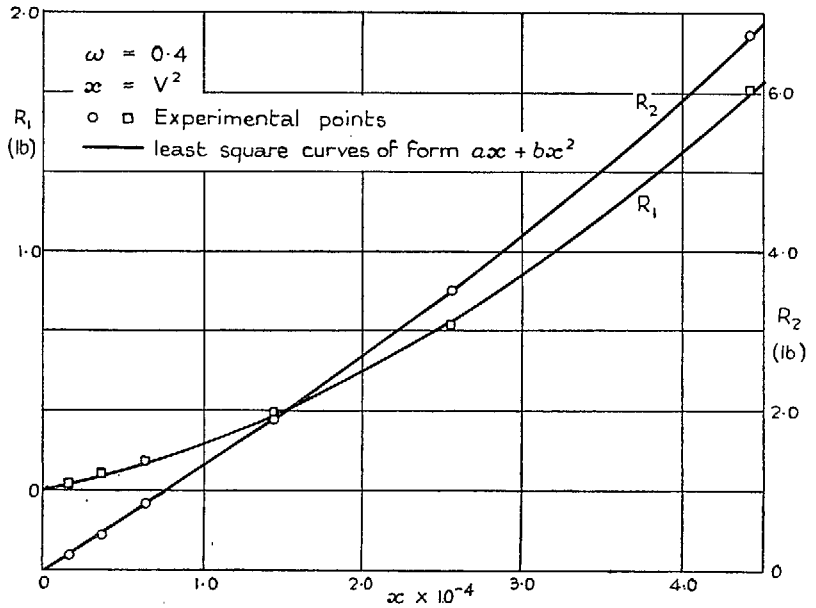

FIG. 20. Measured reactions for constant ω (swept aerofoil—axis OX).

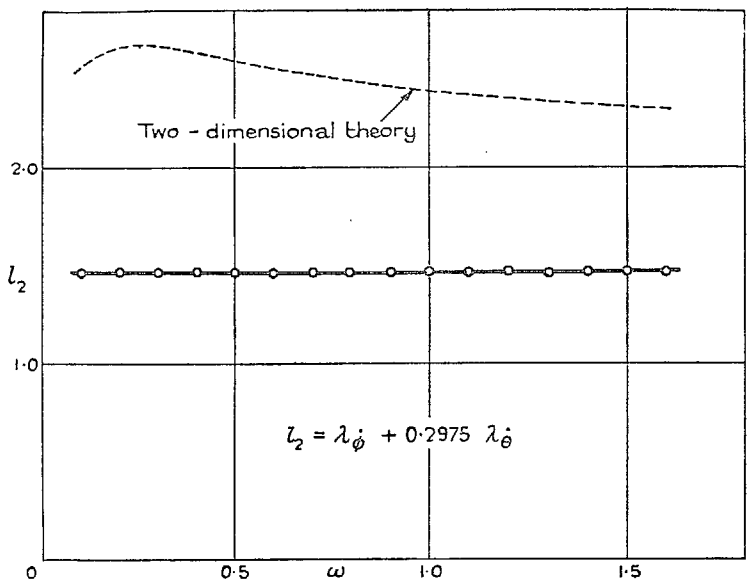

FIG. 21. Dependence of l_2 on ω (swept aerofoil—axis OY).

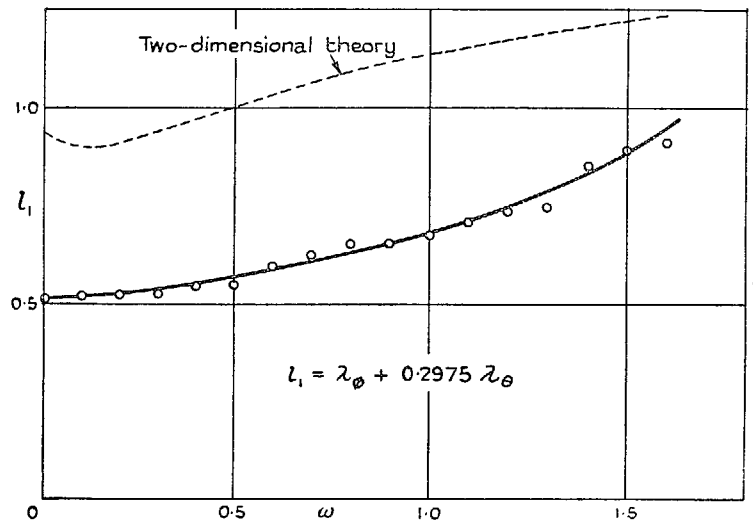

FIG. 22. Dependence of l_1 on ω (swept aerofoil—axis OY).

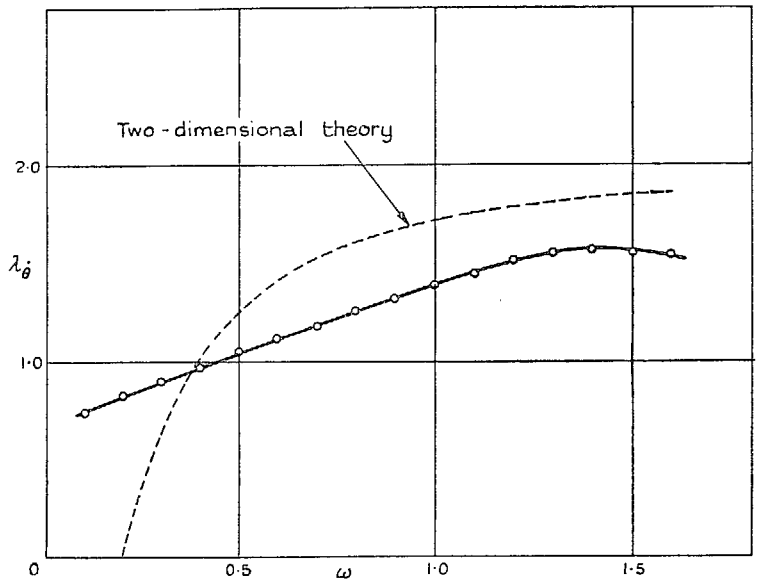

FIG. 23. Dependence of $\lambda_{\dot{\theta}}$ on ω (swept aerofoil—axis OY).

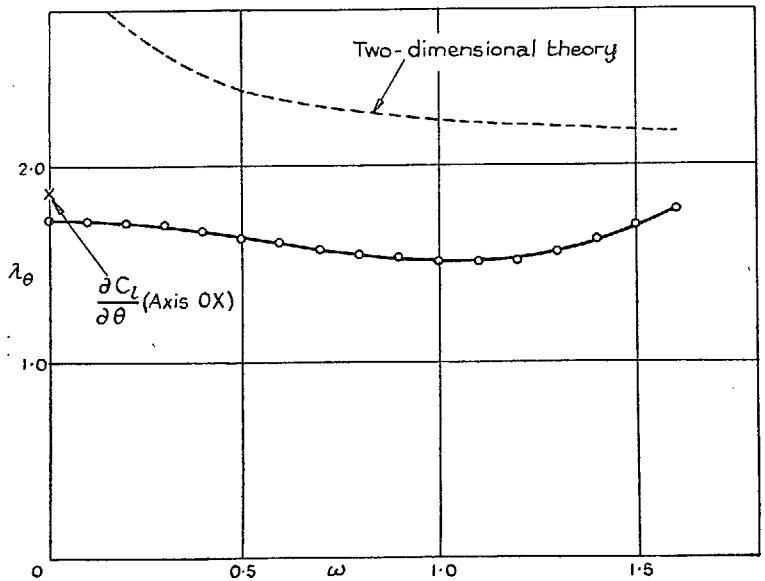

FIG. 24. Dependence of λ_θ on ω (swept aerofoil—axis OY).

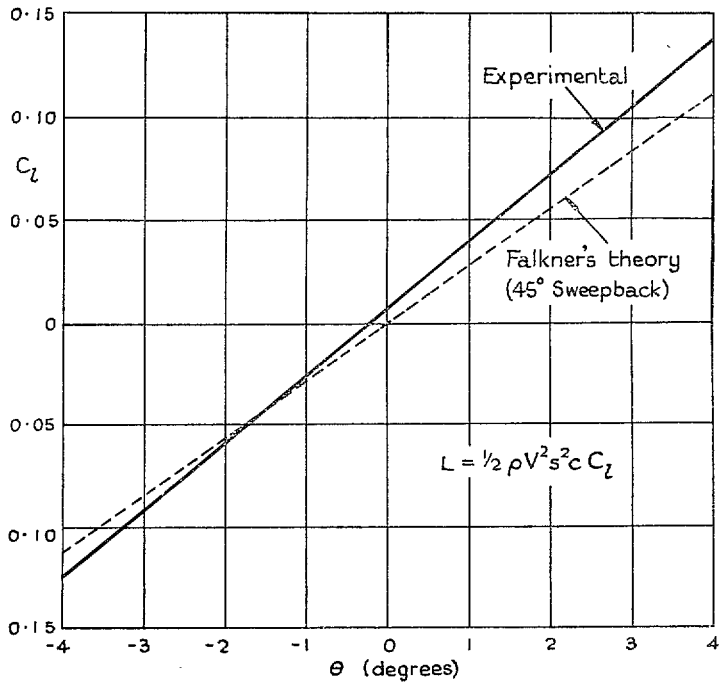

FIG. 25. Variation of C_l with θ (swept aerofoil—axis OX).

Wt. 16/680 K.9 6/53 G.G. 34-262

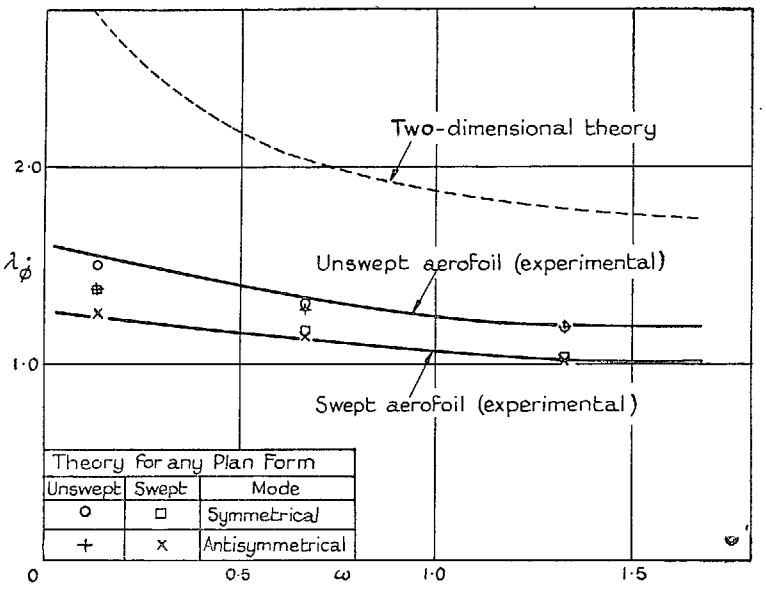

FIG. 26. Comparison with theory for $\lambda_{\dot{\phi}}$.

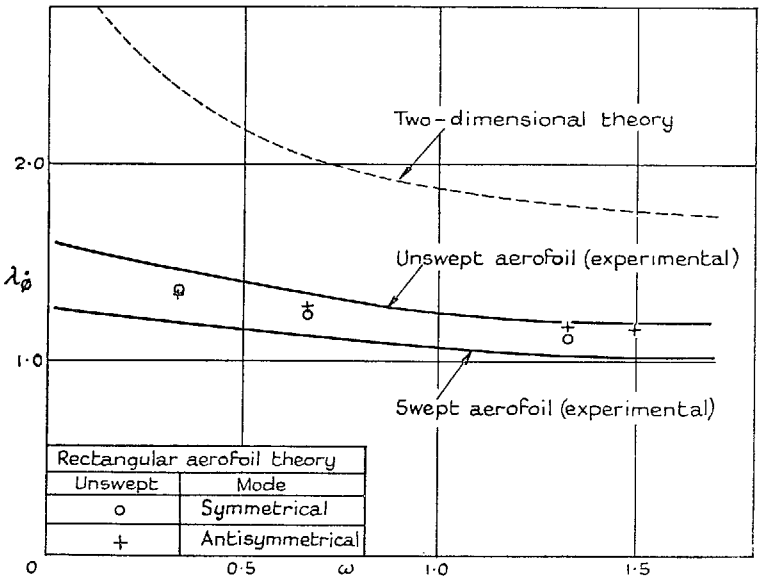

FIG. 28. Comparison with theory for $\lambda_{\dot{\phi}}$.

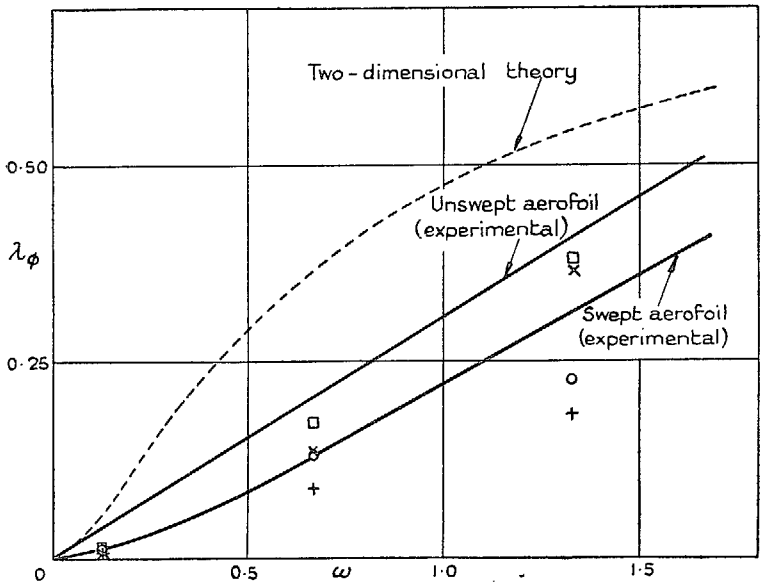

FIG. 27. Comparison with theory for λ_{ϕ}.

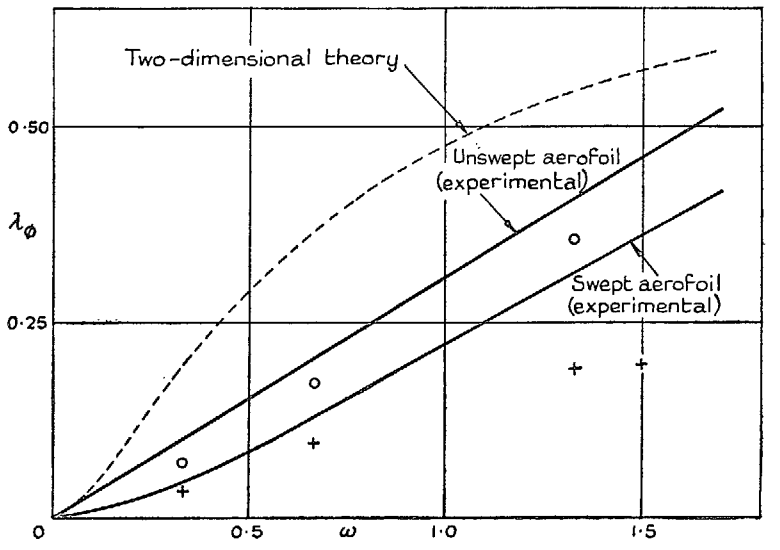

FIG. 29. Comparison with theory for λ_{ϕ}.

PRINTED IN GREAT BRITAIN

Publications of the Aeronautical Research Council

ANNUAL TECHNICAL REPORTS OF THE AERONAUTICAL RESEARCH COUNCIL (BOUND VOLUMES)

1936 Vol. I. Aerodynamics General, Performance, Airscrews, Flutter and Spinning. 40*s*. (40*s*. 9*d*.)
Vol. II. Stability and Control, Structures, Seaplanes, Engines, etc. 50*s*. (50*s*. 10*d*.)

1937 Vol. I. Aerodynamics General, Performance, Airscrews, Flutter and Spinning. 40*s*. (40*s*. 10*d*.)
Vol. II. Stability and Control, Structures, Seaplanes, Engines, etc. 60*s*. (61*s*.)

1938 Vol. I. Aerodynamics General, Performance, Airscrews. 50*s*. (51*s*.)
Vol. II. Stability and Control, Flutter, Structures, Seaplanes, Wind Tunnels, Materials. 30*s*. (30*s*. 9*d*.)

1939 Vol. I. Aerodynamics General, Performance, Airscrews, Engines. 50*s*. (50*s*. 11*d*.)
Vol. II. Stability and Control, Flutter and Vibration, Instruments, Structures, Seaplanes, etc. 63*s*. (64*s*. 2*d*.)

1940 Aero and Hydrodynamics, Aerofoils, Airscrews, Engines, Flutter, Icing, Stability and Control, Structures, and a miscellaneous section. 50*s*. (51*s*.)

1941 Aero and Hydrodynamics, Aerofoils, Airscrews, Engines, Flutter, Stability and Control, Structures. 63*s*. (64*s*. 2*d*.)

1942 Vol. I. Aero and Hydrodynamics, Aerofoils, Airscrews, Engines. 75*s*. (76*s*. 3*d*.)
Vol. II. Noise, Parachutes, Stability and Control, Structures, Vibration, Wind Tunnels. 47*s*. 6*d*. (48*s*. 5*d*.)

1943 Vol. I. (In the press.)
Vol. II. (In the press.)

ANNUAL REPORTS OF THE AERONAUTICAL RESEARCH COUNCIL—

1933–34	1*s*. 6*d*. (1*s*. 8*d*.)	1937	2*s*. (2*s*. 2*d*.)
1934–35	1*s*. 6*d*. (1*s*. 8*d*.)	1938	1*s*. 6*d*. (1*s*. 8*d*.)
April 1, 1935 to Dec. 31, 1936	4*s*. (4*s*. 4*d*.)	1939–48	3*s*. (3*s*. 2*d*.)

INDEX TO ALL REPORTS AND MEMORANDA PUBLISHED IN THE ANNUAL TECHNICAL REPORTS, AND SEPARATELY—

April, 1950 .. .. R. & M. No. 2600. 2*s*. 6*d*. (2*s*. 7½*d*.)

AUTHOR INDEX TO ALL REPORTS AND MEMORANDA OF THE AERONAUTICAL RESEARCH COUNCIL—

1909–1949 .. .. R. & M. No. 2570. 15*s*. (15*s*. 3*d*.)

INDEXES TO THE TECHNICAL REPORTS OF THE AERONAUTICAL RESEARCH COUNCIL—

December 1, 1936 — June 30, 1939	R. & M. No. 1850.	1*s*. 3*d*. (1*s*. 4½*d*.)
July 1, 1939 — June 30, 1945	R. & M. No. 1950.	1*s*. (1*s*. 1½*d*.)
July 1, 1945 — June 30, 1946	R. & M. No. 2050.	1*s*. (1*s*. 1½*d*.)
July 1, 1946 — December 31, 1946	R. & M. No. 2150.	1*s*. 3*d*. (1*s*. 4½*d*.)
January 1, 1947 — June 30, 1947	R. & M. No. 2250.	1*s*. 3*d*. (1*s*. 4½*d*.)
July, 1951	R. & M. No. 2350.	1*s*. 9*d*. (1*s*. 10½*d*.)

Prices in brackets include postage.

Obtainable from

HER MAJESTY'S STATIONERY OFFICE

York House, Kingsway, London, W.C.2; 423 Oxford Street, London, W.1 (Post Orders: P.O. Box 569, London, S.E.1); 13a Castle Street, Edinburgh 2; 39 King Street, Manchester 2; 2 Edmund Street, Birmingham 3; 1 St. Andrew's Crescent, Cardiff; Tower Lane, Bristol 1; 80 Chichester Street, Belfast,
OR THROUGH ANY BOOKSELLER